AGU PUBLICATIONS

Geophysical Research Letters

RESEARCH LETTER

10.1002/2014GL060971

Key Points:
- Explains the major observed features of Titan's dune
- Titan's dunes are still active, elongating westward as finger-like structures
- Sets a new methodology for analyzing sand seas

Supporting Information:
- Readme
- Text S1

Correspondence to:
A. Lucas,
antoine.lucas@cea.fr

Citation:
Lucas, A., et al. (2014), Growth mechanisms and dune orientation on Titan, *Geophys. Res. Lett.*, *41*, doi:10.1002/2014GL060971.

Received 26 JUN 2014
Accepted 12 AUG 2014
Accepted article online 18 AUG 2014

Growth mechanisms and dune orientation on Titan

Antoine Lucas[1], Sébastien Rodriguez[1], Clément Narteau[2], Benjamin Charnay[3], Sylvain Courrech du Pont[4], Tetsuya Tokano[5], Amandine Garcia[1], Mélanie Thiriet[1], Alexander G. Hayes[6], Ralph D. Lorenz[7], and Oded Aharonson[8]

[1]AIM CEA-Saclay, Paris VII-Denis Diderot University, Paris, France, [2]Institut de Physique du Globe de Paris, Sorbonne Paris Cité, University Paris Diderot, UMR 7154 CNRS, Paris, France, [3]LMD IPSL, Paris, France, [4]Laboratoire Matière et Systèmes Complexes, Sorbonne Paris Cité, Université Paris Diderot, CNRS UMR 7057, Paris, France, [5]Institut für Geophysik und Meteorologie Universität zu Köln, Cologne, Germany, [6]Astronomy Division, Cornell University, Ithaca, New York, USA, [7]Johns Hopkins University Applied Physics Lab, Laurel, Maryland, USA, [8]Weizmann Institute of Science, Rehovot, Israel

Abstract Dune fields on Titan cover more than 17% of the moon's surface, constituting the largest known surface reservoir of organics. Their confinement to the equatorial belt, shape, and eastward direction of propagation offer crucial information regarding both the wind regime and sediment supply. Herein, we present a comprehensive analysis of Titan's dune orientations using automated detection techniques on nonlocal denoised radar images. By coupling a new dune growth mechanism with wind fields generated by climate modeling, we find that Titan's dunes grow by sediment transport on a nonmobile substratum. To be fully consistent with both the local crestline orientations and the eastward propagation of Titan's dunes, the sediment should be predominantly transported by strong eastward winds, most likely generated by equinoctial storms or occasional fast westerly gusts. Additionally, convergence of the meridional transport predicted in models can explain why Titan's dunes are confined within ±30° latitudes, where sediment fluxes converge.

1. Introduction

Dune fields are among the most striking landscapes discovered by the Cassini spacecraft on Titan, Saturn's largest moon [*Lorenz et al.*, 2006]. Believed to be made of complex organic sediment, dunes cover more than 17% of the moon's surface, constituting the largest known surface reservoir of organics [*Sotin et al.*, 2012; *Rodriguez et al.*, 2014]. Titan's sand seas were first identified in 2005 by the Cassini-RADAR imager [*Lorenz et al.*, 2006]. As of June 2014, the coverage of Titan by high-resolution synthetic aperture radar (SAR) images (~300 m) has reached 43% of Titan's surface and 60% of its equatorial belt [*Rodriguez et al.*, 2014]. These data show that the vast majority of Titan's dune fields are confined between the tropics within ±30° latitudes. Dunes are linear in shape, often straight over more than a hundred kilometers, with crestlines roughly parallel to the equator with some local variations. In addition, dune terminations and morphologies around topographic obstacles suggest an eastward propagation as shown in Figure 1 [*Lorenz et al.*, 2006]. This interpretation challenges most general circulation models (GCM), which commonly predict easterly winds at low latitudes during a Titan year, which lasts 29.5 Earth years [*Tokano*, 2008; *Lebonnois et al.*, 2012; *Mitchell et al.*, 2011]. Hence, the eastward dune propagation has been intensively discussed [*Lorenz et al.*, 2006; *Lorenz and Radebaugh*, 2009; *Tokano*, 2010; *Charnay et al.*, 2013; *Tokano*, 2008; *Radebaugh et al.*, 2008; *Radebaugh*, 2013; *Radebaugh et al.*, 2010; *Rubin and Hesp*, 2009] and different models for the dune-forming winds have been proposed: (1) an obtuse bimodal wind regime and noncohesive sediment [*Tokano*, 2008], (2) a unidirectional wind regime with noncohesive sediment [*Radebaugh et al.*, 2008], or (3) a cohesive or stabilized sediment in a unidirectional wind regime [*Rubin and Hesp*, 2009]. In addition, it has been recently proposed that strong westerly gusts can be generated during the equinox [*Tokano*, 2010; *Charnay et al.*, 2013], especially in the wake of tropical methane storms, such as those observed in September and October 2010 [*Turtle et al.*, 2011]. Those westerly winds are thought to be strong enough to dominate sediment transport and explain the eastward elongation of Titan's dunes [*Tokano*, 2010; *Charnay et al.*, 2013].

Recent numerical simulations [*Zhang et al.*, 2012], laboratory experiments [*Courrech du Pont et al.*, 2014], and field measurements [*Ping et al.*, 2014; *Courrech du Pont et al.*, 2014; *Lancaster and McCarley-Holder*, 2013] show that, under the same multidirectional wind regime, dunes can have two different orientations depending on sediment availability. In the case of an "infinite" sediment supply, dune growth can be described as a

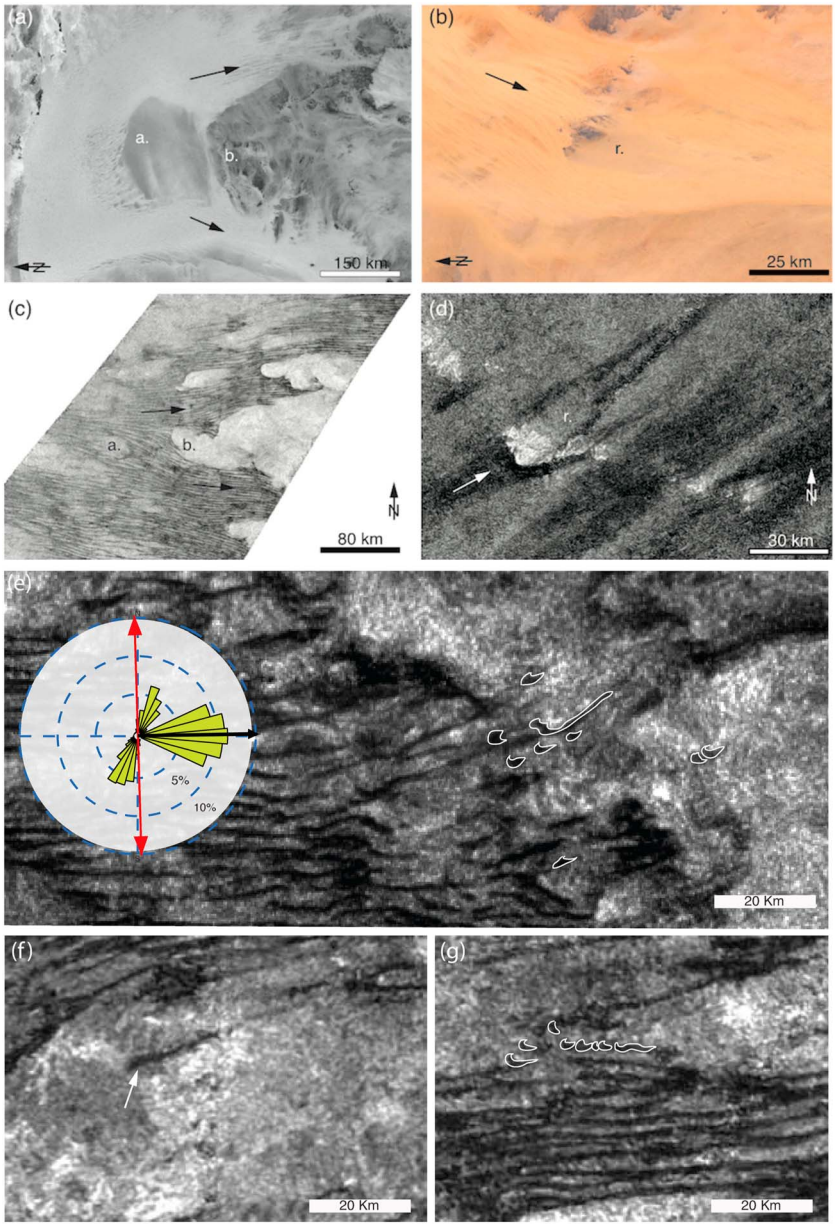

Figure 1. Examples of denoised SAR images of Titan's dune fields to be compared with examples on Earth. (a, b) Dunes interact with local topographic obstacles in Egypt and Libya. (c, d) Examples on Titan from T21 (6.4°N; 80°E and 15°N; 86°E, respectively). "a." indicates absence of the primary patterns; "b." indicates local topographic obstacles. Shadowing effect of the flow behind obstacle is shown with "r." letters, allowing to predict the direction of propagation highlighted by the arrows. (e) Barchanoids and seif-like dunes observed on T3 (13°N; 106°W), (f) Dune forming under the fingering mode on T21 (2.8°N; 76°E). (g) Barchanoids seen on T21 (8.3°N; 79°E). On each panel, interdunes are characterized by brighter backscatter suggesting either no or small amount of sediment. Inset in Figure 1e shows the sediment fluxes and predicted crest orientations for the bed instability (red arrows) and the fingering mode (black arrow) accounting for the storm (see main text for details). For clarity only one rose is displayed, but they all show very similar patterns for Figures 1a and 1b and 1e–1g.

bed instability that selects the alignment for which the gross bed form-normal transport is maximum [*Rubin and Hunter*, 1987] (henceforth referred to as the bed instability mode). In contrast, recent work [*Reffet et al.*, 2010; *Courrech du Pont et al.*, 2014] shows that for the case of a limited sediment supply where dunes grow by the transport of sediment over a nonerodible bed, finger-like structures extend in the direction of the resultant sediment flux (henceforth referred to as the fingering mode). Thus, sediment availability controls the dune growth mechanism and the subsequent dune trend. Most importantly for our present

purpose, the method commonly used to derive dune orientation from wind data [*Rubin and Hunter*, 1987] has been recently refined by taking into account these two dune growth mechanisms and their corresponding orientations [*Courrech du Pont et al.*, 2014; *Fenton et al.*, 2014] (see supporting information). For a given wind regime, there are therefore two distinct dune orientations that correspond to these two different growth mechanisms. By coupling predicted wind regimes to observed dune patterns, one can potentially distinguish between them and determine the dominant dune growth mechanism on Titan using available GCMs [*Tokano*, 2010; *Charnay et al.*, 2013] with a data set that has been improved by image processing [*Lucas et al.*, 2014].

2. Observations From Cassini SAR Images

High-resolution SAR images acquired between October 2004 and June 2013 have been inspected to isolate individual dune features [*Lorenz et al.*, 2006; *Rodriguez et al.*, 2014]. However, these images suffer from speckle noise, which hinders advanced geomorphic analysis and automatic processing. In order to remove the speckle [*Lucas et al.*, 2014], which is inherent to SAR processing, we applied a Non-Local Denoising (NLD) algorithm to the SAR images. The resulting NLDSAR images provide a significant improvement for the identification and mapping of geomorphic structures, especially for features at the limit of the SAR resolution such as the dune crests, dune widths, and interdune areas (see a comparison between SAR and NLDSAR in the supporting information). In particular, NLDSAR images show that Titan's linear dunes present a "nail-head" shape from which they elongate and thin from the eastern side of an obstacle (Figures 1a and 1d). In both Martian and terrestrial linear dunes, this behavior is characteristic of dunes emerging from a pile of sediment accumulating behind a topographic obstacle and elongating away from the source (eastward in Titan's case). This confirms the suspicion from broader-scale analysis of dune deviation around topographic anomalies [*Lorenz and Radebaugh*, 2009]. Asymmetric barchans with eastward arms and seif dunes (i.e., sinuous linear dunes) are also found [*Ewing et al.*, 2013; *Radebaugh et al.*, 2010; *Radebaugh*, 2013], generally at the edge of dune fields (Figures 1a and 1d), providing additional morphological evidences for an eastward dune elongation at all latitudes and longitudes (Figures 1d, 1e, and 1g).

The use of NLDSAR images improves the efficacy of automatic processing techniques [*Lucas et al.*, 2014]. With the aim to extract dune orientation at regional scales, we used a linear segment detection (LSD) algorithm [*Grompone von Gioi et al.*, 2012] over all the dune fields identified on a global RADAR map of Titan [*Rodriguez et al.*, 2014] (Figure 2). Upon visual inspection of all segments detected on the NLDSAR images, false dune crest detections (i.e., $< 0.5\%$) were removed. Ultimately, this method allowed extracting tens of thousands individual segments associated with Titan's dune crests by using both SAR and NLDSAR images (see supporting information). This automatic detection correctly retrieves the local deviations within the dune fields. Therefore, one segment provides a specific orientation at local scale. North-south variations averaged in longitude are controlled to the first order by the climatic general circulation, which is not affected by either topography or albedo contrasts. Therefore, using all of the LSD segments within zonal bands, we obtained the latitudinal distribution of dune orientation (Figure 3a). Globally, we see that Titan's dune orientations are closely parallel to the equator with a minor polarward direction of propagation in both hemispheres that rarely exceeds $\pm 20°$. Second-order deviations are also observed at higher-spatial frequency with smaller amplitudes. These deviations are distributed over the entire equatorial band and may be associated with local forcing on dune orientation such as mesoscale topography and the subsequent recirculation flows [*Lorenz et al.*, 2013].

3. Predictions From Climatic Modeling

3.1. Climatic Models

To compare the observed dune orientations to those predicted by the two dune growth mechanisms (i.e., the bed instability and the fingering modes), we used near surface winds extracted from different climatic models: (i) the Institut Pierre-Simon Laplace (IPSL)-Laboratoire de Météorologie Dynamique (LMD) GCM for Titan [*Lebonnois et al.*, 2012], (ii) the Cologne Titan GCM [*Tokano*, 2008] which is able to generate occasional fast westerly gusts during equinoxes [*Tokano*, 2010], and (iii) the coupling between a mesoscale model [*Barth and Rafkin*, 2007] and the IPSL-LMD GCM for Titan [*Lebonnois et al.*, 2012; *Charnay et al.*, 2013]. Note that the lowest-level model is located at 35 m above the surface for models (i) and (iii) and 300 m for model (ii) but results are extrapolated to the surface by using a logarithmic boundary layer assumption [*Charnay et al.*, 2013]. All climatic models take into account the seasonal variability due to Titan's obliquity and Saturn's

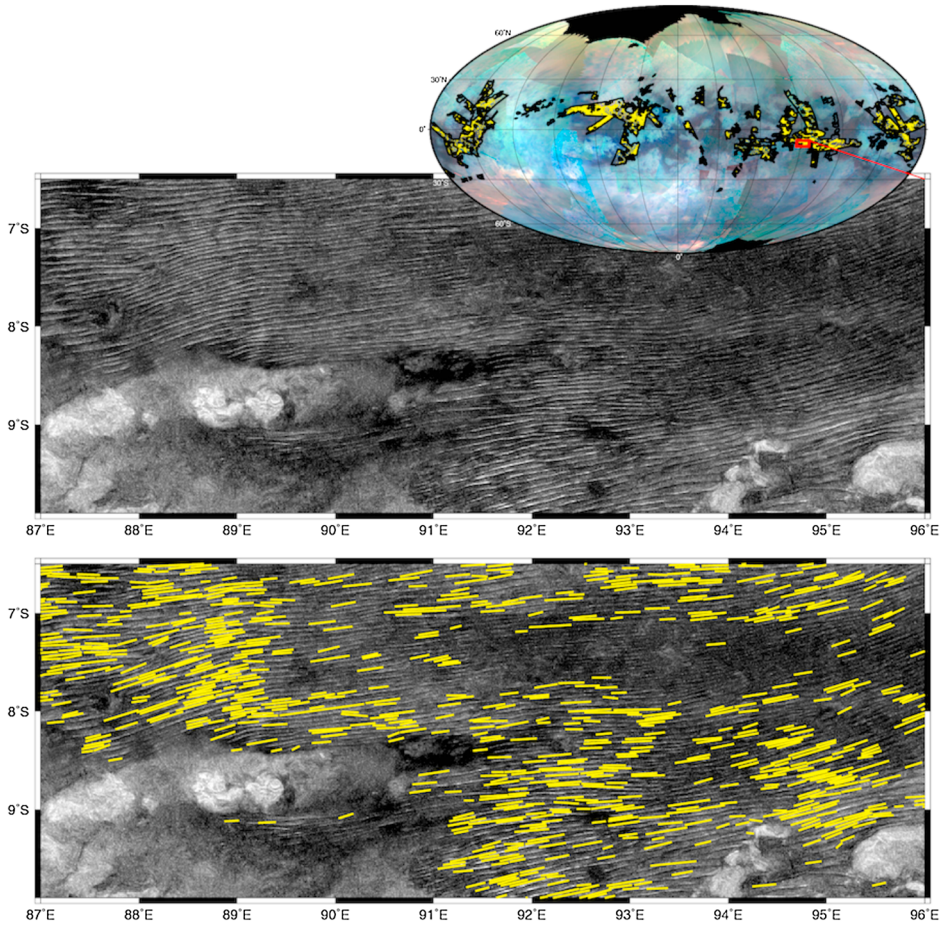

Figure 2. Linear segment detection over Titan's dune fields. (Inset) Visual and infrared mapping spectrometer (VIMS) global map with extracted segments in yellow. Black polygons contour the dune fields mapped from SAR images (including TA through T92). The red box indicates the location of the close-up of NLDSAR release of T8 shown below with and without the segment overlays shown in yellow. Note that as dunes can extend in some cases hundreds of kilometers continuously, they can incorporate multiple individual segments.

nonzero eccentricity. The mesoscale model [*Barth and Rafkin*, 2007] is used to simulate strong eastward gusts produced by equinoctial storm events [*Turtle et al.*, 2011], which are taken into account in model (iii) [*Charnay et al.*, 2013]. Finally, we document wind variability over an entire Titan year using a GCM grid of 3° in latitude and 11° in longitude. The output of the second climatic model [*Tokano*, 2008, 2010] is provided with higher sampling frequency (i.e., seven hundreds) but only at a few specific locations (e.g., 0° and ±30° of latitude).

3.2. Crestline Orientation and Growth Mechanisms

From the wind data and sediment transport law from *Ungar and Haff* [1987], adapted to Titan's conditions [*Lorenz et al.*, 1995], we calculated sediment fluxes and the dune orientations associated with the two growth mechanisms [*Courrech du Pont et al.*, 2014] for the three climatic models (see supporting information). Sediment fluxes are estimated using the following: a friction speed threshold of 0.04 m s^{-1}, a particle diameter of 200 μm with a density of 1000 kg m^{-3}, an air density of 5.3 kg m^{-3} [*Charnay et al.*, 2013]. This leads to a threshold speed of 1 m s^{-1}. As for the storms we take a frequency of 0.1 event/equinox with a latitudinal spreading of 20° centered at the equator [*Charnay et al.*, 2013]. The resulting latitudinal distributions of the two predicted dune orientations are shown in Figure 3. Under climatic models (i) and (ii), neither of the two growth mechanisms are able to predict the observed orientations (Figure 3a). The difference between the observed and the predicted orientations is larger than 30° and 20° at all latitudes for models (i) and (ii), respectively. Qualitatively, both models predict the same trend for the bed instability crest orientation (i.e., anticorrelated with observations). In case of model (i), the common seasonal winds are easterly

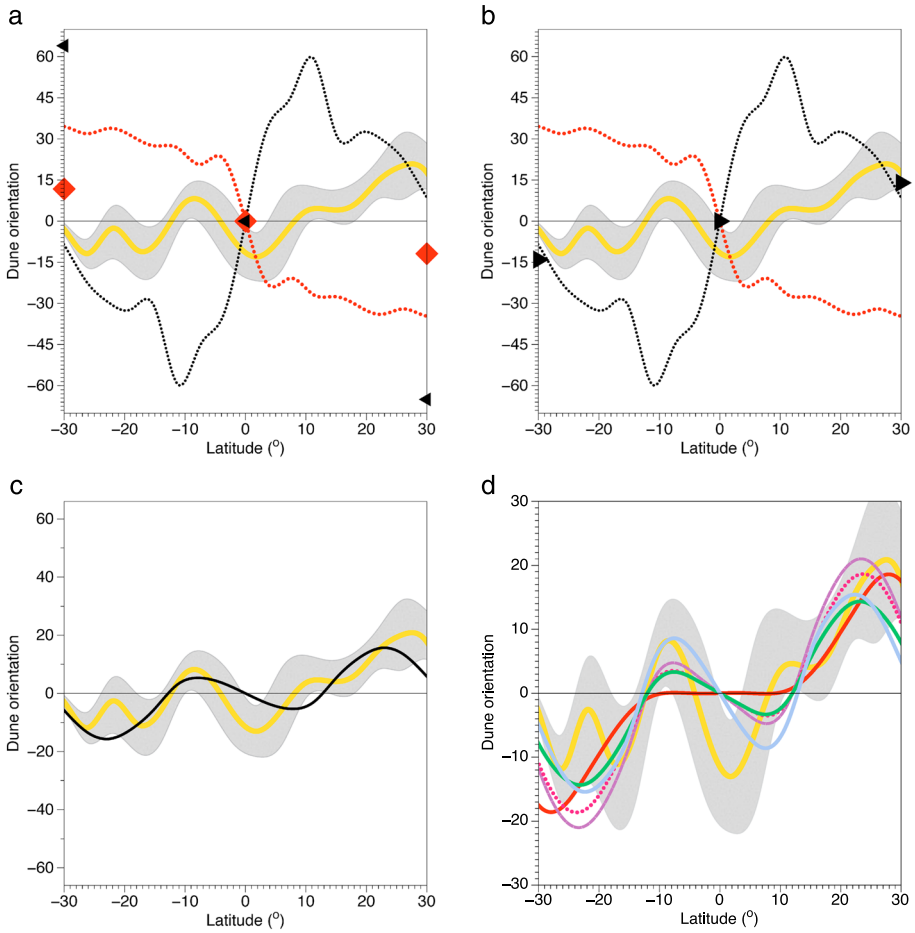

Figure 3. Observed and predicted dune orientation with respect to latitudes. The mean value of the observed dune orientation distribution is shown in yellow. The standard deviation interval of this distribution is shown in gray. All orientations are measured anticlockwise from east. (a–c) Predicted orientations for the bed instability and the fingering modes are shown in red and black, respectively. For the nominal parameters (see main text), Figure 3a shows the prediction from climatic models (i) and (ii) in dashed lines and symbols respectively. Figure 3b shows the prediction from climatic model (ii) with a larger velocity threshold (1.4 m s^{-1}) is shown. Note that in that case, the bed instability mode falls outside of the range. Figure 3c shows the prediction from climatic model (iii) accounting for the equinoctial storms. The fingering mode is shown in black. Note that the bed instability mode (red symbols) while accounting for the storms falls outside of the range and is therefore not shown here. Figure 3d shows the sensitivity test for storm properties: close-up on the fingering mode between ±30° of deviation: $u^*_{th} = 0.04$, $S_f = 0.15$, $S_s = 20°$ (red), $u^*_{th} = 0.031$,$S_f = 0.21$ (violet), $S_s = 20°$, $u^*_{th} = 0.032$, $S_f = 0.3$, $S_s = 20°$ (red dashed), $u^*_{th} = 0.032$, $S_f = 0.3$ (green), $S_s = 25°$, and $u^*_{th} = 0.03$, $S_f = 0.25$, $S_s = 25°$ (bright blue).

and cannot account for the eastward propagation of the dunes. In case of model (ii), while bed instability crest orientation predictions are not too far from observations, the fingering mode indicates a westward propagation, in disagreement with observations. A threshold speed of 1.4 m s^{-1} selects only westerly gusts, leading to a net eastward sediment flux, although the average equatorial surface wind is easterly [*Tokano*, 2010]. Consequently, associated crest orientations for the fingering mode predicted under such conditions lead to a better agreement with the observation as shown in Figure 3b. This agreement is also true for the eastward sediment propagation, which concords with previous discussions [*Tokano*, 2010].

In the third climatic model, which is model (i) with the effect of equinoctial storms on sediment transport, we find that the predicted dune orientations change significantly compared to model (i). While the bed instability mode still fails to reproduce the observed dune alignments, the fingering mode quantitatively agrees with the observations (Figure 3c). Indeed, the predicted dune trends of this mode are within one standard deviation of the observed dune orientation distribution at all latitudes. As all of the parameters considered in this third climatic model suffer from uncertainties, we test the sensitivity of the predicted

dune orientations by varying the total sediment flux associated with storms (frequency and size), and the friction speed threshold (Figure 3d). For the fingering mode, all of our tests show the same latitudinal behavior for dune orientation with only slight differences in amplitude, which are mainly controlled by the storms' contribution. These results are similar to the primary calculation and thus to the observations. Indeed, all the cases shown fall within/or close to the observed distribution interval (Figure 3d).

Ultimately, the fingering mode of dune growth matches the observations (Figure 3). Upon closer inspection, we observed that dunes are clearly aligned with the resultant drift directions, whereas the bed instability mode generally generates dunes that are oblique to the resultant transport direction (Figures 2e–2g, and supporting information). Such dunes shift sideway that creates defects so that they look like barchanoid ridges (see Figure 1e). In contrast, Titan dunes extend coherently on large distances what argues for a fingering mode of growth in the direction of the resultant sediment flux.

Therefore, our results support that either the occasional fast westerly gusts [*Tokano*, 2010] or the equinoctial storms [*Charnay et al.*, 2013] are at the origin of the eastward propagation of the dunes. In either case, the bed instability mode does not satisfy the observations for the considered wind regimes, while the fingering mode is the only one which can explain the current dunes' orientation and direction of propagation.

3.3. Sediment Fluxes and Sand Seas Confinement

The model implies that, outside the dunes, there is a limited amount of mobilized sediment on Titan's surface. The bed of potentially mobile particles in the interdune is probably thin and is not likely to constitute a reservoir from which the dune can grow in height. This provides new constraints on the sediment properties in the interdune areas, and more generally, on Titan's global sediment supply [*Rodriguez et al.*, 2014]. High-resolution VIMS observations show that substrate is detectable within the interdunes [*Barnes et al.*, 2008] suggesting a depleted sediment supply. Nominal VIMS observations (with lower spatial resolution) integrate the contributions of both sediment and potential substrate with a fraction of about two thirds and one third, respectively, also in good agreement with RADAR observations [*Rodriguez et al.*, 2014]. As for the RADAR observations themselves, backscatter contrast values suggest that sediment could be present in between dunes (Figures 2c and 2d) while depleted interdunes are also observed (Figures 2e–2g, and supporting information). Terrestrial analogs found in Egypt suggest that either the sediment is nonerodible/nonmobilized or secondary dunes form from this available sediment supply and therefore grow in height following the bed instability crest orientation [*Courrech du Pont et al.*, 2014]. Such secondary patterns on Titan would be an order of magnitude smaller and therefore could not be resolved by the RADAR.

Consequently, dunes morphodynamics are compatible with the seasonal variability of current wind models, which suggests that dunes may be still active today.

These results shed a new light on the mechanisms for eastward dune propagation [*Rubin and Hesp*, 2009]. Models implying a unidirectional wind regime are unlikely on Titan [*Lebonnois et al.*, 2012] and are not in agreement with observed orientations. The storm-driven eastward gusts recently proposed [*Charnay et al.*, 2013] imply a multidirectional wind regime. Note that such storms have been observed during the last equinox [*Turtle et al.*, 2011].

From the sediment fluxes predicted by our climatic models, we can also compute the divergence of the flux $\mathbf{Q}$ to estimate, from the equation of conservation of mass, where zones of erosion ($\nabla.\mathbf{Q} > 0$) and deposition ($\nabla.\mathbf{Q} < 0$) occur (Figure 4a). Our calculations indicate that at latitudes of 15°N/S the divergence reaches a maximum and the meridional sediment flux vanishes. As meridional sediment flux divides at 15°N/S, the convergence of the sediment flux toward the equator turns this equatorial band into a major aeolian sediment trap at the scale of Titan. This is in qualitative agreement with the observed geographic distribution of the dune fields and dune material (i.e., brown unit on Figure 4b) [*Rodriguez et al.*, 2014].

4. Conclusion

Accounting for two dune growth mechanisms and independent climatic models, we accommodated all the documented features of Titan's dunes in one self-consistent scenario. Dune orientation and dune field location are quantitatively constrained providing new insights on the largest surface hydrocarbon's reservoir on Titan. Furthermore, we show that, like many dune fields on Earth [*Lancaster*, 2010], dunes on Titan are consistent with the fingering mode.

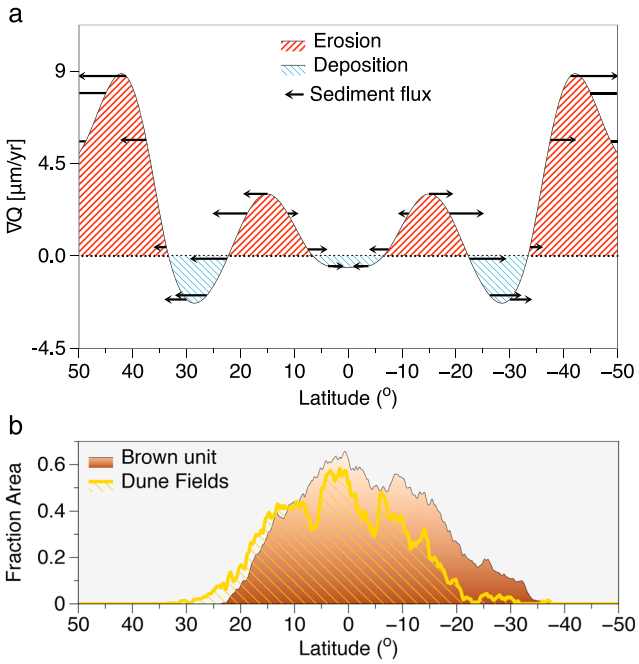

Figure 4. Divergence of sediment flux and dune segregation on Titan. (a) Latitudinal sediment flux divergence using the output of climatic model (iii). Zones of erosion and deposition are shown in red and blue, respectively. Latitudinal component of the sediment fluxes is represented by the black arrows (i.e., vector modulus is a log function of the flux). (b) Latitudinal distribution of dunes and sediments (i.e., brown unit) (adapted from *Rodriguez et al.* [2014]). The sediment fluxes show an accumulation zone in the tropical region (±30°), which corresponds to the IR brown unit distribution [*Rodriguez et al.*, 2014].

Finding sediment sources is a key issue regarding the development of dune fields, especially when differentiating dunes in the fingering mode from dunes in the bed instability mode. This is even more important considering that in many cases on Earth, the interdune area of dunes in the fingering mode may contain sediment and exhibit sand sheets of segregated coarse grains [*Dong et al.*, 2008; *Courrech du Pont et al.*, 2014]. Unfortunately, sediment supply, availability, and mobility are strongly unconstrained on Titan, and the SAR images do not allow to determine these quantity accurately. For example, isolated sediment sources may exist on Titan but remain to be discovered. Another possibility would be that Titan's dunes are old enough to have formed longitudinally from initial sources that have now disappeared.

As proposed in *Charnay et al.* [2013] and discussed here, the sediment must be dominantly transported by strong eastward winds, most likely generated by equinoctial events. In addition, their climatic model can also explain the tropical confinement where all sediment fluxes converge. This scenario also implies that, while a few isolated examples of fossilized dunes exist as proposed by *Radebaugh* [2013], dunes on Titan are for the most part consistent with the current wind regime. Finally, our model does not need to invoke cohesive sediment properties to explain the growth of Titan's dunes, although such a mechanism cannot be ruled out [*Rubin and Hesp*, 2009].

Acknowledgments

Authors thank the Nvidia Academic Hardware Donation Program, the Agence Nationale de la Recherche (ANR Projects EXODUNES 12BS05001, France), the UnivEarthS Labex program at Sorbonne Paris Cité (ANR-10-LABX-0023 and ANR-11-IDEX-0005-02), and the Space Campus program from Université Paris-Diderot. A.L. acknowledges the CNES for supporting this research. R.L. acknowledges support from NASA via grant NNX13AH14G. Authors thank the two anonymous reviewers for their constructive comments. Shapefiles and climatic outputs can be obtained upon request to the corresponding author.

The Editor thanks Nick Lancaster and an anonymous reviewer for their assistance in evaluating this paper.

References

Barnes, J. W., et al. (2008), Spectroscopy, morphometry, and photoclinometry of Titan's dunefields from Cassini/VIMS, *Icarus*, *195*(1), 400–414.

Barth, E. L., and S. C. R. Rafkin (2007), TRAMS: A new dynamic cloud model for Titan's methane clouds, *Geophys. Res. Lett.*, *34*, L03203, doi:10.1029/2006GL028652.

Charnay, B., et al. (2013), Methane storms control Titan's dune orientation, Abstract P53D-1893, presented at 2010 Fall Meeting, AGU, San Francisco, Calif., 13–17 Dec.

Courrech du Pont, S., C. Narteau, and X. Gao (2014), Two modes for dune orientation, *Geology*, doi:10.1130/G35657.1.

Dong, Z., et al. (2008), Pseudo-feathery dunes in the Kumtagh desert, *Geomorphology*, *100*, 328–334.

Ewing, R. C., A. G. Hayes, and A. Lucas (2013), Reorientation time-scales of Titan's equatorial dunes, *Lunar and Planetary Institute Science Conference Abstracts, 44*, 1187, Houston, Tex.

Fenton, L. K., T. I. Michaels, and R. A. Beyer (2014), Inverse maximum gross bedform-normal transport 1: How to determine a dune-constructing wind regime using only imagery, *Icarus*, *230*, 5–14.

Grompone von Gioi, R., J. Jakubowicz, J.-M. Morel, and G. Randall (2012), LSD: A line segment detector, *Image Processing On Line*, *2*, 35–55, doi:10.5201/ipol.2012.gjmr-lsd.

Lancaster, N. (2010), Assessing dune-forming winds on planetary surfaces-application of the gross bed form normal concept, *In Second International Planetary Dunes Workshop*, Alamosa, Colo.

Lancaster, N., and G. McCarley-Holder (2013), Decadal-scale evolution of a small dune field: Keeler dunes, California, 1944–2010, *Geomorphology*, *181*, 281–291.

Lebonnois, S., J. Burgalat, P. Rannou, and B. Charnay (2012), Titan global climate model: A new 3-dimensional version of the IPSL Titan GCM, *Icarus*, *218*(1), 707–722.

Lorenz, R. D., and J. Radebaugh (2009), Global pattern of Titan's dunes: Radar survey from the Cassini prime mission, *Geophys. Res. Lett.*, *36*, L03202, doi:10.1029/2008GL036850.

Lorenz, R. D., J. I. Lunine, J. A. Grier, and M. A. Fisher (1995), Prediction of aeolian features on planets: Application to Titan paleoclimatology, *J. Geophys. Res.*, *100*(E12), 26,377–26,386.
Lorenz, R. D., et al. (2006), The sand seas of Titan: Cassini radar observations of longitudinal dunes, *Science*, *312*(5774), 724–727.
Lorenz, R. D., et al. (2013), A global topographic map of Titan, *Icarus*, *225*(1), 367–377.
Lucas, A., et al. (2014), Insights into Titan's geology and hydrology based on enhanced image processing of Cassini RADAR data, *J. Geophys. Res. Planets*,, doi:10.1002/2013JE004584.
Mitchell, J. L., M. Dmkovics, R. Caballero, and E. P. Turtle (2011), Locally enhanced precipitation organized by planetary-scale waves on Titan, *Nat. Geosci.*, *4*, 589–592.
Ping, L., C. Narteau, Z. Dong, Z. Zhang, and S. Courrech du Pont (2014), Emergence of oblique dunes in a landscape-scale experiment, *Nat. Geosci.*, *7*(2), 99–103.
Radebaugh, J. (2013), Dunes on Saturn's moon Titan as revealed by the Cassini mission, *Aeolian Res.*, *11*, 23–41.
Radebaugh, J., et al. (2008), Dunes on Titan observed by Cassini radar, *Icarus*, *194*(2), 690–703.
Radebaugh, J., R. Lorenz, T. Farr, P. Paillou, C. Savage, and C. Spencer (2010), Linear dunes on Titan and Earth: Initial remote sensing comparisons, *Geomorphology*, *121*(1-2), 122–132.
Reffet, E., S. Courrech du Pont, P. Hersen, and S. Douady (2010), Formation and stability of transverse and longitudinal sand dunes, *Geology*, *38*, 491–494.
Rodriguez, S., et al. (2014), Global mapping and characterization of Titan's dune fields with Cassini: Correlation between RADAR and VIMS observations, *Icarus*, *230*, 168–179.
Rubin, D. M., and P. A. Hesp (2009), Multiple origins of linear dunes on Earth and Titan, *Nat. Geosci.*, *2*, 653–658.
Rubin, D. M., and R. E. Hunter (1987), Bedform alignment in directionally varying flow, *Science*, *237*, 276–278.
Sotin, C., et al. (2012), Observations of Titan's northern lakes at 5μm: Implications for the organic cycle and geology, *Icarus*, *221*(2), 768–786.
Tokano, T. (2008), Dune-forming winds on Titan and the influence of topography, *Icarus*, *194*(1), 243–262.
Tokano, T. (2010), Relevance of fast westerlies at equinox for the eastward elongation of Titan's dunes, *Aeolian Res.*, *2*(2-3), 113–127.
Turtle, E. P., et al. (2011), Rapid and extensive surface changes near Titan's equator: Evidence of April showers, *Science*, *331*(6023), 1414–1417.
Ungar, J. E., and P. K. Haff (1987), Steady state saltation in air, *Sedimentology*, *34*, 289–299.
Zhang, D., C. Narteau, O. Rozier, and S. Courrech du Pont (2012), Morphology and dynamics of star dunes from numerical modelling, *Nat. Geosci.*, *5*(7), 463–467.